Ocean Engineering 123 (2016) 346–356

Contents lists available at ScienceDirect

Ocean Engineering

journal homepage: www.elsevier.com/locate/oceaneng

Accounting for ship manoeuvring motion during propeller selection to reduce CO_2 emissions

D.G. Trodden *, M.D. Woodward, M. Atlar

School of Marine Science and Technology, Armstrong Building, Newcastle University, Newcastle upon Tyne NE1 7RU, United Kingdom

ARTICLE INFO

Article history:
Received 1 July 2015
Received in revised form
5 July 2016
Accepted 6 July 2016
Available online 26 July 2016

Keywords:
Simulation
Optimisation
Design-point
Unsteady flow
Propeller modelling
Manoeuvring

ABSTRACT

The aim of this research is to reduce Carbon Dioxide emission through enhanced propeller selection achieved by a more realistic identification of the true propeller operating point. By recognising that the 'dead-ahead steady speed in flat calm water' condition is not representative of the true operation of a ship in a seaway, a new paradigm is proposed. By taking into consideration the effects of wind and waves on the ship's true speed through the water and thus the probable load condition of the propeller, throughout the ship's mission, a probable propeller operating condition is identified. Propellers are then selected for both the original condition and the adapted condition, and their performance compared using time-domain mission simulations. The objective of the study is to demonstrate how the alternative propeller selection methodologies proposed, can on average provide greater overall efficiency.

Results from the case studies are encouraging, with a gain of 2.34% in open water propeller efficiency for a 3600 Twenty foot Equivalent Unit container ship, equating to a saving of 3.22% in Carbon Dioxide emissions.

1. Introduction

In 2012 it was estimated that about 2.2% of the world's anthropogenic Carbon Dioxide (CO_2) emissions were from ship's exhausts, and that CO_2 was the most important GHG in terms of quantity and global warming potential (MEPC, 2014). With international trade steadily increasing (World Trade Organization, 2013), an increased demand for global shipping brings with it escalating CO_2 emissions and related environmental problems. The IMO are enforcing measures upon the shipping fleet's CO_2 production, aiming at a reduction of 30% by the year 2025.

To address the problem of CO_2 abatement, this research aims at reducing CO_2 emissions through increased efficiency from designing propellers around *service conditions*. Ship's are commonly optimised around a specific design point, but frequently operated away from this point, resulting in loss of efficiency. Reasons for operating the ship away from her design point are numerous and diverse, ranging from running a heavily loaded propeller due to increased hull fouling, to operating procedure as dictated by the shipping company. It is the intent of this research to focus on optimised propeller selection. To elucidate the term *propeller selection* in this context: this is the process of selecting an optimised propeller from a standard series.

A ship will be subjected to forces and moments from the natural environment in which she is sailing. The ship's response to these forces and moments affects the flow field around the ship, and hence the loading on the propeller.

In order to achieve a more realistic in-service design point, the manoeuvring motions of surge, sway and yaw have been accounted for in the process of selecting a suitable ship's propeller. To simplify the methodology, the initial development of this research concentrates on the manoeuvring motion, rather than combined manoeuvring and seakeeping motions. It is thought that the manoeuvring motion will have the most influence over results, as the average of these motions' velocities are likely to be non-zero, whereas in the seakeeping motions, averaged velocities are likely to be near zero (with perhaps the exception of roll). This research further assumes that the propeller remains deeply submerged.

Simulation of a ship's manoeuvring motion has been examined by various people, including the whole-ship type approach of Abkowitz (1964), and the modular approach used by Hirano (1981) and Oltmann and Sharma (1984). These techniques solve a series of Ordinary Differential Equations (ODEs) in the time domain. There also exist several techniques to model unsteady flow on propeller action, for example Boundary Element Methods (BEM) or Panel Methods (Kerwin et al., 1987), including cavitation prediction (Young and Kinnas, 2001), or from Field Methods such as Unsteady Reynolds Average Navier–Stokes (URANS) methods (Dubbioso et al., 2013; Li et al., 2015). In order to simulate the unsteady action of a propeller during a manoeuvre, or when

* Corresponding author.
E-mail addresses: david.trodden@ncl.ac.uk (D.G. Trodden), michael.woodward@ncl.ac.uk (M.D. Woodward), mehmet.atlar@ncl.ac.uk (M. Atlar).

http://dx.doi.org/10.1016/j.oceaneng.2016.07.002

Nomenclature

α	propeller section angle of incidence to flow (rad)
α_E	effective propeller's section angle of incidence to flow (rad)
α_{ss}	Propeller's section angle of incidence at which static stall occurs (rad)
η_o	open water propeller efficiency (–)
Δ_P	pitch rate, or reduced frequency (–)
δ	ship's drift angle (rad)
ξ	foil section leading edge suction recovery factor (–)
ρ	density (kg $m^{-3)}$
σ	cavitation number (–)
$\phi(s)$	Wagner function
χ	wake skew angle (rad)
ψ	propeller blade azimuth angle (rad)
ω	frequency of oscillation (rad s^{-1})
BAR	Blade Area Ratio
c	chord of propeller blade at localised section (m)
CBEMT	Combined Blade Element Momentum Theory
C_D	coefficient of drag (–)
C_L	coefficient of lift (–)
CO_2	Carbon Dioxide
D	propeller diameter (m)
DWT	deadweight tonnage (t)
GHG	Green House Gas
HFO	Heavy Fuel Oil
ISO	International Organisation for Standardisation
I_{zz}	mass moment of inertia about the Z-axis (kg m^2)
J	propeller advance coefficient (–)
KCS	Kriso Container Ship
K_Q	propeller torque coefficient (–)
K_T	propeller thrust coefficient (–)
L_{PP}	length between perpendiculars (m)
m	mass (kg)
N	moment of yaw (N m)
n	propeller's rotational speed (revolutions s^{-1})
ODE	Ordinary Differential Equation
OOVOO	propeller action model as described by Oosterveld and van Oossanen (1975).
P	nominal pitch of propeller (m)
P_Δ	non-dimensionalised pitch rate (–)
P_B	engine brake power (kW)
PID	Proportional Integral Derivative (controller)
P_o	static water pressure at propeller's shaft centreline (N m^{-2})
P_v	vapour pressure at localised propeller section (N m^{-2})
Q	torque (N m)
R	radius of propeller (m)
r_P	radius of propeller at localised section (m)
r	yaw rate [rad s^{-1}]
SiS	Ship in Service (simulator)
SFC	Specific Fuel Consumption (g/kW h)
T	thrust (N)
t	time (s)
TEU	Twenty-foot Equivalent Unit container
u	surge velocity (m s^{-1})
v	sway velocity (m s^{-1})
V_i	induced velocity (m s^{-1})
V_v	resulting ship's velocity (s^{-1})
V_p^*	total resulting velocity vector across a propeller's blade element
V_a	propeller's speed of advance (m s^{-1})
V_∞	freestream velocity (m s^{-1})
VLCC	Very Large Crude Carrier
X	force in surge direction (N)
Y	force in sway direction (N)
Z	number of blades on propeller (–)

sailing in a seaway, the propeller model needs to be executed at least every time-step of the manoeuvring simulation. Conventional unsteady propeller codes would take a prohibitively long time to run, therefore a novel modification to the computationally fast Combined Blade-Element Momentum Theory (*CBEMT*) (Carlton, 1997) approach has been taken and adapted to include altered dynamic lift and drag coefficients arising from oblique, unsteady inflow.

To analyse the effects of the propeller on the action of the rudder, and thereby the ships's manoeuvrability, velocity changes over the rudder due to the contraction of the race and relative inflow angle, can be accounted for using schemes from, for example Kose et al. (1981). Generally when concerned with the study of manoeuvring, the direct effects of propeller action on sway and yaw are neglected (Yoshimura, 2005). Indeed, there appears to be little in the literature in the way of effects of manoeuvring on propeller performance, or vice versa, propeller action on manoeuvring. This paper addresses that gap.

In conventional propeller selection, flow vectors at a particular polar coordinate on the propeller plane are assumed to be constant with time, and thus neglect manoeuvring motion. This paper details a method for accounting for this unsteady flow, and incorporating it within a ship manoeuvring simulation.

While various people, including Glauert (1928) and Coleman et al. (1945) developed techniques to account for steady effects of oblique flow within the *CBEMT*, and McCroskey (1981), Green and Galbraith (1994) and Shen and Fuhs (1999) were developing methods to explore and account for dynamic operation on lift and drag components, it is not thought that these techniques have previously been incorporated together. This paper highlights the techniques involved in this incorporation.

A ship manoeuvring simulator, named the *Ship in Service* (SiS) simulator, has been developed which models the unsteady motion response of a ship and her propulsion plant to environmental loading, and is thus able to analyse propeller and propulsion performance, including CO_2 emissions from ships in diverse voyage scenarios.

2. The effects of the environment on ship manoeuvring

The environmental forces and moments considered in this study arise from wind, waves and surface currents. These environmental forces and moments will tend to push a ship off of her desired course.

If the effects of the environmental loading result in a ship sailing with some drift angle, there are five subsequent consequences that may develop:

1. The ship has now attained a sway velocity; the drag vector of which must be added to the forward resistance. The ship must then travel at an amended forward speed if it is to reach its destination in the same overall time.
2. There is also a change in the forward resistance to account for, due to the new flow pattern around the ship, resulting in a modified form coefficient.

3. If rudder action is required to check any yawing moments, then an induced drag from the rudder will also add to the ship's overall resistance.
4. The flow pattern into the propeller will be modified due to the ship's new attitude in the water.
5. The environment itself will be imparting additional forces and moments on the ship, resulting in a change in resistance.

The above aspects are modelled in the developed mathematical model, explained in the next section.

3. Mathematical model

There are numerous mathematical models which can be found in the open literature, that are capable of representing the action of a propeller, and the manoeuvring response of a ship, however, the effect that the manoeuvring motion has on the action of the propeller is not so well established.

Some of the more pertinent requirements of a simulator for use as an early design tool are:

1. Simulation should be computationally fast.
2. Require only a modest amount of input detail.
3. Have enough fidelity to model aspects of the design which significantly affect performance.

The approach taken in the development of the simulator used in this study, is to solve a series of differential equations in the time domain. While being a relatively fast way to solve the equations of motion, it will be shown to include enough fidelity to model unsteady, non-linear velocity inflow into a propeller, caused by the action of a ship's manoeuvring response to environmental loading.

3.1. Equations of motion

It can be shown that the equations of motion in surge, sway and yaw, with the origin located at the centre of gravity, can be written as follows:

$$m(\dot{u} - rv) = X_H + X_R + X_P + X_W + X_A \quad \text{Surge} \tag{1a}$$

$$m(\dot{v} + ru) = Y_H + Y_R + Y_P + Y_W + Y_A \quad \text{Sway} \tag{1b}$$

$$I_{zz}\dot{r} = N_H + N_R + N_P + N_W + N_A \quad \text{Yaw} \tag{1c}$$

where m is the mass of the ship, I_{zz} is the mass moment of inertia around a vertical axis. u and v are the ship's velocity in pure surge and sway respectively, and r is the ship's rate of change of heading. The subscripts H, R, P, W and A in Eq. (1), denote hull, rudder, propeller, waves and wind respectively. The methodologies used to estimate these contributions are briefly discussed next.

3.2. Hull

The method to model the longitudinal force, transverse force and yawing moment on the hull, X_H, Y_H, and N_H respectively, is described in Inoue et al. (1981).

3.3. Rudder

The calculation for the longitudinal force (drag) X_R, transverse force, Y_R and turning/yawing moment N_R imposed upon the ship by the action of the rudder follows the scheme of Lee et al. (2003). When an order for the rudder to be put over is given, the rudder does not instantaneously arrive at the given order, but takes a certain amount of time. The electromotive oil pressure steering gear model of Son (1989) is used to account for this time lag. The equation is solved simultaneously with the other equations of motion to obtain the rudder angle at a particular time step.

3.4. Environmental forces and moments

The forces and moments imposed on a ship due to the wind are obtained using the method as described by Blendermann (1996). An unsteady wind velocity model is incorporated into the developed simulator using the Davenport (1978) spectrum for the variation in the longitudinal component of the wind due to gusting.

The method of Townsin et al. (1992) is used to estimate the longitudinal force imposed on a ship from encountering waves at any angle. It is considered as a basis for further development, which gives a representative value for added wave resistance.

Surface currents are accounted for using the principle of relative motion, that is, the speed of the ship with respect to a point on Earth is equal to the velocity of the ship minus the velocity of the current. It is assumed that the surface current has no velocity gradient along the length of the ship, and that the speed of the current is constant.

3.5. Automatic pilot

In order for the simulated ship to maintain course and speed, as would be the case in a real-world scenario, an automatic pilot is implemented to compensate for any speed and course deviations arising from environmental influences. The autopilot consists of two Proportional, Integral, Derivative (PID) controllers, one for course keeping and another for speed keeping.

3.6. Engine and propeller dynamics

The main propulsion engine is assumed to be a directly coupled slow speed two-stroke Diesel engine.

The telegraph order sets the rate of propeller revolutions. This is achieved by altering the rate of fuel flow into the engine, thereby altering the torque the engine produces. The difference between the resisting torque of the water on the propeller and the output torque from the engine results in the acceleration of the drive train.

3.7. Propeller

Two propeller models are used in the analysis of this study. The first neglects the effects of manoeuvring motion, that is, the inflow is assumed to arrive from directly in-front of the propeller, and is based on the work of Oosterveld and van Oossanen (1975). For the sake of brevity, this model is denoted the *OOVOO* model in this text. The model also does not account for the effects of pure sway or yaw imparted to the ship by the propeller's action.

The second propeller model accounts for the ship's manoeuvring motion and is based on a modified Combined Blade-Element Momentum Theory (*CBEMT*) model.

3.7.1. Wake and thrust deduction factor

The wake at the propeller plane for a ship at zero drift angle, w_{P0} and thrust deduction factor, *tdf* are calculated from the analysis carried out by Holtrop (1984).

Eq. (2), from the work of Hirano (1981), is used to estimate the wake fraction at the propeller plane:

$$w_P = w_{P0}\exp\left(-4.0\beta_P^2\right) \tag{2}$$

where the drift angle at the propeller, β_P is given by the following equation:

$$\beta_P = \arcsin\left(\frac{v + x_P r}{V_v}\right) \tag{3}$$

x_P is the distance of the x-coordinate of the propeller from midships (a negative value $\approx -0.5L_{pp}$), and V_v is the resultant ship speed.

Throughout the analysis, the ship is operating within the first quadrant, that is, an ahead rotational speed, and ahead speed of advance, and as such, the thrust deduction factor is assumed to be a constant. A method to correct for thrust deduction fraction in different quadrants can be found in Harvald (1967).

3.7.2. The OOVOO propeller model

This model is used as a calibration tool for the modified *CBEMT* model to ensure that identical propellers are chosen in calm-water conditions, independent of the model used for selection by the propeller selection algorithm (Section 4.1). Being a well established model, it also serves as a model to compare results with. Expressions for the thrust and torque coefficients, K_T and K_Q respectively on a B-Screw Series propeller are obtained from the methods described in Oosterveld and van Oossanen (1975). The calculation scheme for the longitudinal force, X_P, transverse force, Y_P and yawing moment, N_P follows that of Eq. (4).

$$X_P = \left(1 - tdf\right)\rho n^2 D^4 K_T \tag{4a}$$

$$Y_P \approx 0 \tag{4b}$$

$$N_P \approx 0 \tag{4c}$$

where ρ is water density, n is propeller rotational speed and D is propeller diameter.

3.7.3. The modified CBEMT unsteady propeller model

A description of the standard *CBEMT* method can be found in most books on propellers, e.g. Carlton (1997). The *CBEMT* method was chosen as a basis to adapt and model propeller action, as it is computationally fast and can easily be adapted to include extra functionality. The *CBEMT* method in its original form does not take into account flow arriving at an oblique angle to the propeller plane, as would happen if a ship is travelling at some drift angle. It is this drift angle, as calculated from the manoeuvring simulation module which is used to calculate the modified and varying inflow vectors to the propeller. The following paragraphs elucidate the fundamental modifications made to both the Blade-Element and General Momentum theories in order to account for oblique flow, and follow the general scheme as described in Stettler (2004).

Overview of modifications to fundamental general momentum theory: When adapting the General Momentum Theory to account for oblique flow, the hypothesis of Glauert (1928) (cf. Fig. 1) was used to calculate the flow velocity at the disc, as per Eq. (5), which is used in turn for the thrust and torque calculations in the original theory.

$$V = \sqrt{V_a^2 + 2V_i V_a \cos\delta + V_i^2} \tag{5}$$

V_a is the speed of advance, V_i is induced velocity and δ is an arbitrary angle to the free-stream known as the drift angle.

To account for tip loss present in a finite number of blades, the method described in Goldstein (1929) is employed.

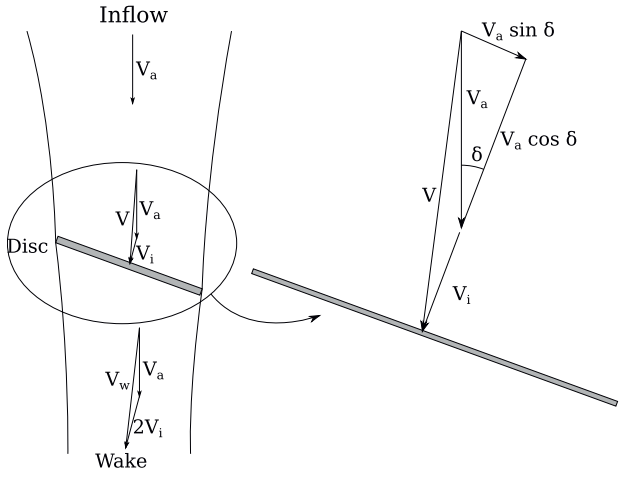

Fig. 1. Glauert's concept of a helicopter rotor in oblique flow.

Overview of modifications to fundamental blade-element theory: The present methodology uses a linearised expression for the distribution of induced velocity from theory originally developed by Coleman et al. (1945), and shown in the following equation:

$$V_i = V_{i0}\left[1 + \frac{r_p}{R}\tan\left(\frac{\chi}{2}\right)\cos\psi\right] \tag{6}$$

V_{i0} is the mean induced velocity (i.e. at the centre of the disc), r_p is the radial coordinate on the disc, ψ is the azimuthal angle, χ is the wake skew angle in the downstream direction, which is directly related to the ship's drift angle, as depicted in Fig. 2. This approach is used to calculate the modified disc-averaged in-plane (or cross-flow) and axial induced velocities for each blade section element.

Conventionally, the coefficients for lift and drag used in *CBEMT* neglect any unsteady effects, however, a propeller's blade is now accelerating towards and away from the incoming (oblique) flow. This acceleration results in modified sectional lift and drag coefficients, and stall angles. Shen and Fuhs (1999) developed a method which conglomerated a variety of approaches to account for unsteady flow, and produced a practical mechanism to estimate sectional lift and drag coefficients in fully attached, transitional and fully separated flow. It is these sectional lift and drag coefficients that are used in the current modified *CBEMT* unsteady propeller model.

In order to obtain values for lift and drag coefficients, C_L and C_D respectively, arising from unsteady flow, a term which defines the degree of unsteadiness is required (Leishman, 2002). This term is denoted the Pitch Rate, Δ_P, also referred to as Reduced Frequency, and is defined in the following equation:

$$P_\Delta = \frac{\dot{\alpha}c}{2V_\infty} \tag{7}$$

$\dot{\alpha}$ is the time derivative of angle of attack, c is the chord length of foil section, and V_∞ is upstream flow velocity.

The angle of attack for each blade element section is directly related to the ship's instantaneous drift angle and propeller geometry, the details of which can be found in Trodden (2014), thus relating drift angle to Pitch Rate.

3.7.4. Dynamic lift

The following expressions are obtained from Shen and Fuhs (1997, 1999).

Fully attached flow:

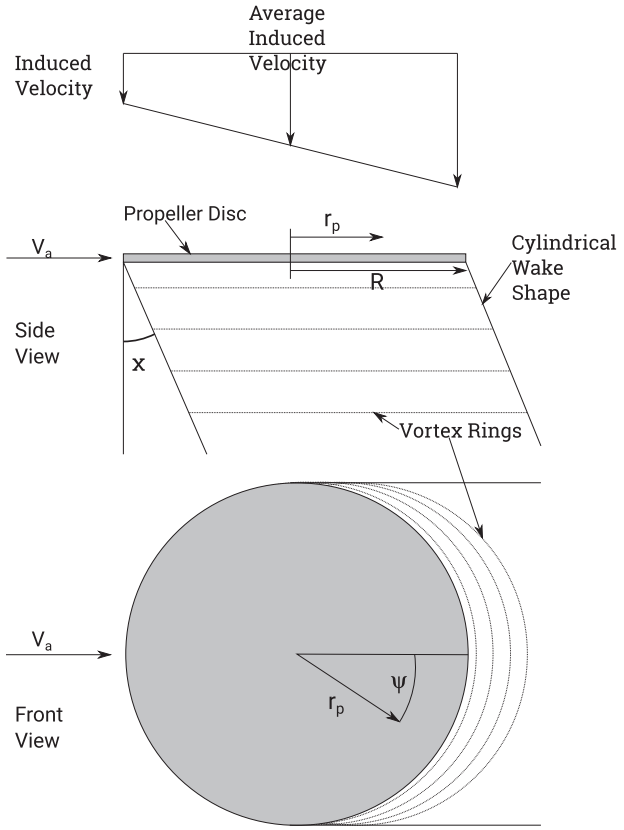

Fig. 2. Distribution of induced velocity across propeller disc (Stettler, 2004).

$$C_L = (C_L)_{\text{static}} - \left(\frac{\partial C_L}{\partial \alpha}\right)_{\text{dynamic}} \alpha_w(s) + \text{sign}(\dot{\alpha})\pi P_\Delta \quad \text{for } \alpha \le \alpha_{ss} \tag{8}$$

where α_{ss} is the angle of incidence at which static stall occurs, and $\alpha_w = \alpha - \alpha_E$ accounting for the time history effects of the change in the angle of incidence.

α_E is the effective angle of incidence, and is defined in the following equation:

$$\alpha_E(s) = \alpha(0)\phi(s) + \int \frac{\mathrm{d}\alpha}{\mathrm{d}u}\phi(s-u)\mathrm{d}u \tag{9}$$

$\phi(s)$ is the Wagner function, and s denotes a non-dimensional time parameter, given by: $s = 2V_p^* t/c$. The angle of incidence at which zero lift occurs is denoted $\alpha(0)$. u is a velocity vector which accounts for a phase difference in impulse response.

Leishman and Beddoes (1989) present the following numerical approximation for Duhamel's integral for the effective angle of attack:

$$\alpha_E(s) = \alpha(0)\phi(s) + \sum_{n=1}^{m} \Delta\alpha_n - \mathbb{X}_n - \mathbb{Y}_n \tag{10}$$

where

$$\mathbb{X}_0 = 0 \quad \text{and} \quad \mathbb{X}_n = \mathbb{X}_{n-1}\exp(-b_1\Delta s) + A_1\Delta\alpha_n \tag{11a}$$

$$\mathbb{Y}_0 = 0 \quad \text{and} \quad \mathbb{Y}_n = \mathbb{Y}_{n-1}\exp(-b_2\Delta s) + A_2\Delta\alpha_n \tag{11b}$$

Δs is the distance travelled by the section in semi-chords over a sample interval Δt and $\Delta\alpha_n$ is the corresponding change in angle of attack over that time interval. Beddoes (1976) provides the constants A_1, A_2, b_1 and b_2 to be 0.165, 0.335. 0.0455 and 0.3 respectively.

The Wagner function, $\phi(s)$ can be approximated with sufficient accuracy from Bisplinghoff et al. (1996)

$$\phi(s) = \frac{s+2}{s+4} \tag{12}$$

McLaughlin (1992) compiled an extensive data set of lift slopes for several airfoil sectional profiles. A functional relationship between static and dynamic lift slope can be expressed as:

$$\left(\frac{\partial C_L}{\partial \alpha}\right)_{\text{dynamic}} = 0.94\left(\frac{\partial C_L}{\partial \alpha}\right)_{\text{static}} \tag{13}$$

Values for the static lift slopes may readily be obtained, for example, from the literature (Abbott and Von Doenhoff, 1959), codes such as Drela (2013) or approximations from Prandtl lifting-line theory.

Transitional flow:

$$C_L = (C_L)_{ss} + \left(\frac{\partial C_L}{\partial \alpha}\right)_{\text{static}} (\alpha - \alpha_{ss}) - \left(\frac{\partial C_L}{\partial \alpha}\right)_{\text{dynamic}} \alpha_w(s) + \text{sign}(\dot{\alpha})\pi P_\Delta \quad \text{for } \alpha_{ss} < \alpha \le \alpha_{DM} \tag{14}$$

The dynamic moment stall angle, α_{DM} is the critical angle above which the flow is considered to be fully separated (Shen and Fuhs, 1999), and is defined in Section 3.7.6

Fully separated flow:

$$C_L = \frac{2\pi \sin\alpha}{4 + \pi \sin\alpha}\left[1 + \sigma + \frac{\sigma^2}{8(\pi+4)}\right]\cos\alpha + \text{sign}(\dot{\alpha})\pi P_\Delta \quad \text{for } \alpha > \alpha_{DM} \tag{15}$$

σ is the cavitation number, defined in the following equation:

$$\sigma = \frac{P_o - P_v}{\frac{1}{2}\rho V^2} \tag{16}$$

where P_o is a reference pressure taken as the static pressure at a particular localised blade-element position, P_v is the vapour pressure of the working fluid, and V is the localised fluid velocity.

3.7.5. Dynamic drag

Kottapalli and Pierce (1979) studied the effects of an oscillating airfoil in a fluctuating free stream. This data was further analysed by Leishman (1989) who show that fluctuations in unsteady viscous drag are small and negligible when compared with the pressure drag. It is assumed that friction drag is not frequency dependent, implying that the unsteady effect on the drag force comes from the pressure drag. The dynamic effect on pressure drag is calculated as follows.

Fully attached flow:

$$C_D = C_{DF} + C_{DP} \tag{17}$$

$$C_D = \left[C_{DF} + \frac{1}{2}C_L(1-\xi)\sin(2\alpha)\right]_{\text{static}} + \text{sign}(\dot{\alpha})\pi P_\Delta \cos\alpha \sin\alpha \quad \text{for } \alpha \le \alpha_{ss} \tag{18}$$

where ξ is the leading edge suction recovery factor, accounting for the failure of the foil section to achieve leading edge suction it would have achieved in potential flow. A typical value for ξ is around 0.95–0.97 (Leishman and Beddoes, 1989).

Transitional flow:

$$C_D = \left\{ C_{DF} + \frac{1}{2}\left[(C_L)_{ss} + \left(\frac{\partial C_L}{\partial \alpha}\right)_{\text{static}} (\alpha - \alpha_{ss}) \right](1 - \xi)\sin(2\alpha) \right\}_{\text{static}} + \text{sign}(\dot{\alpha})\pi P_\Delta \cos\alpha \sin\alpha \quad \text{for } \alpha_{ss} < \alpha \le \alpha_{DM} \tag{19}$$

Fully separated flow:

$$C_D = \frac{2\pi \sin\alpha}{4 + \pi \sin\alpha}\left[1 + \sigma + \frac{\sigma^2}{8(\pi + 4)}\right]\sin\alpha + \text{sign}(\dot{\alpha})\pi P_\Delta \cos\alpha \sin\alpha \quad \text{for } \alpha > \alpha_{DM} \tag{20}$$

3.7.6. Criteria used in determining flow regime

The two criteria used in determining the flow regime, as noted in the previous paragraphs are α_{ss} and α_{DM}. Most foil sections have a constant static stall angle of around 15° (Abbott and Von Doenhoff, 1959), and is the value assumed in this analysis. Shen and Fuhs (1999) developed an empirical formula relating the dynamic moment stall angle, α_{DM} with pitch rate from the work done on oscillating foil tests of McCroskey (1981), and the ramp-up tests of Francis and Keesee (1985) and Green and Galbraith (1994). viz.

$$\alpha_{DM} = \begin{cases} \alpha_{ss} + 340 P_\Delta & \text{if } P_\Delta \le 0.03 \\ \alpha_{ss} + 10.2 + 53.5(P_\Delta - 0.03) & \text{if } P_\Delta > 0.03 \end{cases} \tag{21}$$

3.8. Effects of unsteady flow on propeller performance

Fig. 3 is an output as calculated from the *SiS* simulator, showing how the lift coefficient of a blade section varies with non-dimensionalised pitch rate, (P_Δ) (i.e., the degree of unsteadiness in the flow), and clearly shows how the stall angle increases with increasing pitch rate. Drag coefficients can be plotted in a similar manner. Lift coefficient increases with increasing pitch-rate due to the kinematic induced camber effect and unsteady boundary-layer response (Leishman, 2002).

For small drift angles, the angle of attack usually remains below the stall angle. However, as can be seen from the output of the *SiS* simulator in Fig. 4, when the drift angle becomes larger, it starts to become an important aspect, especially for sections near the propeller's root and when examining manoeuvring trials like turning circles.

Lift and drag characteristics of the blade sections, and therefore pitch rate, directly relate to the torque, thrust and cavitation

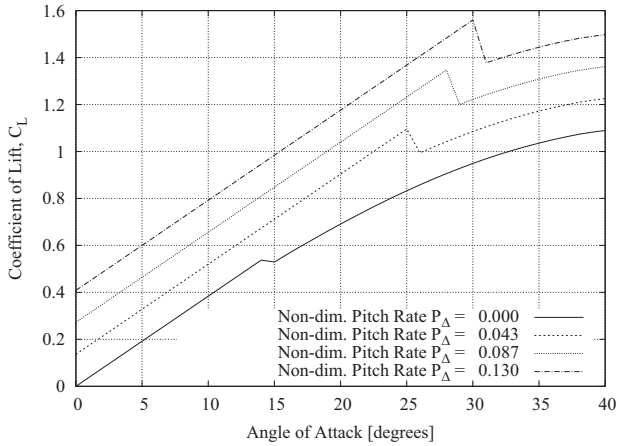

Fig. 3. Lift coefficient vs angle of attack for various non-dimensionalised pitch rate, for given aspect ratio.

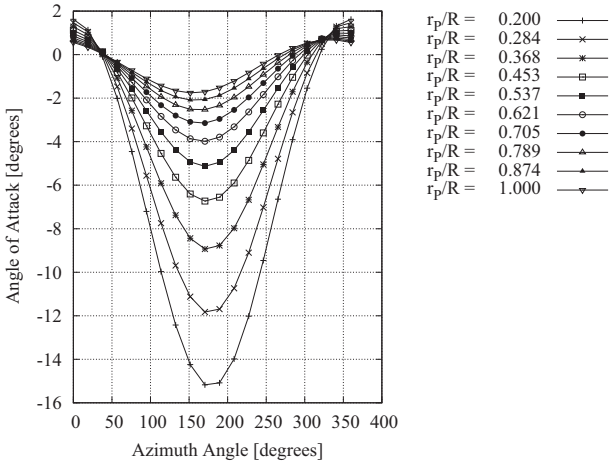

Fig. 4. Angle of attack vs azimuth angle at a drift angle of 13.33°.

properties of the blade. Fig. 5 shows calculations from the *SiS* simulator, depicting how the non-dimensional pitch rate varies, both 'around the clock' and across the radius, The two Fig. 5a and b show in comparison of the difference in magnitude of non-dimensional pitch rate for drift angles of 0.00° and 8.89° respectively.

For comparison, Fig. 6 shows characteristics for the same propeller, as calculated from both the *OOVOO* and modified *CBEMT* methods.

A detailed description of how the components of the modified *CBEMT* model are assembled can be found in Trodden (2014).

4. Analysis procedure

The ODEs developed in Section 3 are solved simultaneously in the time domain via a 4th order Runge–Kutta method. This results in distances, velocities, accelerations and hence forces and moments on the hull, rudder, and on the blade elements of the propeller at a given instant in time.

4.1. An optimum propeller selector

As well as having an analysis sub-programme to obtain propeller performance, the *SiS* simulator has an optimisation routine which will select a basis propeller from a standard B-Screw series, that best suites the route's conditions. This optimisation scheme is described next.

A propeller is first optimised for calm water conditions. The main parameters (number of blades *Z*, Blade Area Ratio *BAR*, and pitch: diameter ratio *P*/*D*) are then run through the simulation. The environmental conditions that the ship experiences are not calm weather and so the propeller's efficiency will not be equal to the initial design. From output of the simulator i.e. required thrust, speed of advance and drift angle at the propeller, a new optimised propeller is chosen. This propeller's parameters are passed to the simulator module and the simulation run again. Because the propeller is different, the output from the simulation will be different, and thus an iterative procedure takes place, until the efficiency from the previous run is within tolerance of the present run.

In order to determine the optimum propeller for each simulation run, it is necessary to obtain the optimum screw rotation rate for a given propeller diameter, knowing the required thrust (obtained from the simulator). The speed of advance at the propeller is also obtained from the simulator.

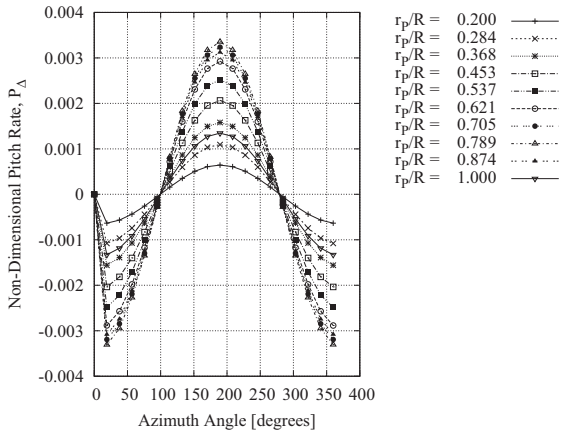

(a) Non-dimensionalised pitch rate vs azimuth angle at a drift angle of 0.00°

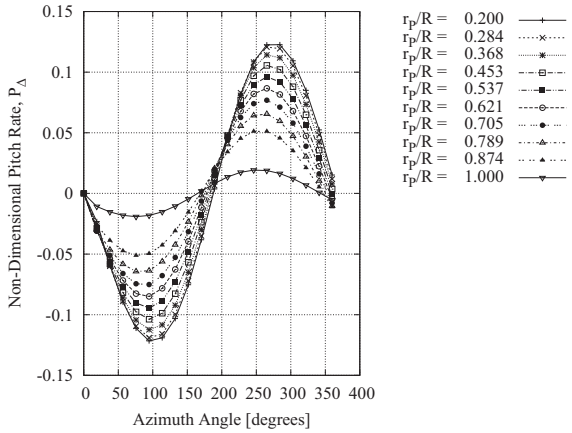

(b) Non-dimensionalised pitch rate vs azimuth angle at a drift angle of 8.89°

Fig. 5. Effect of drift angle on pitch rate of propeller blade sections.

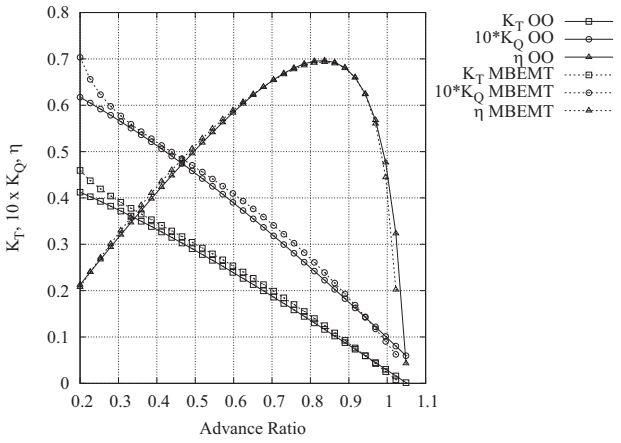

Fig. 6. Comparison plot of *OOVOO* and calibrated unsteady modified *CBEMT* propeller models for *KCS* stock propeller, at zero degree drift angle.

As only the required thrust, propeller diameter and speed of advance are known, the values for K_T and J cannot yet be calculated. However, the value for $\frac{K_T}{J^2}$ can, as from the following equation:

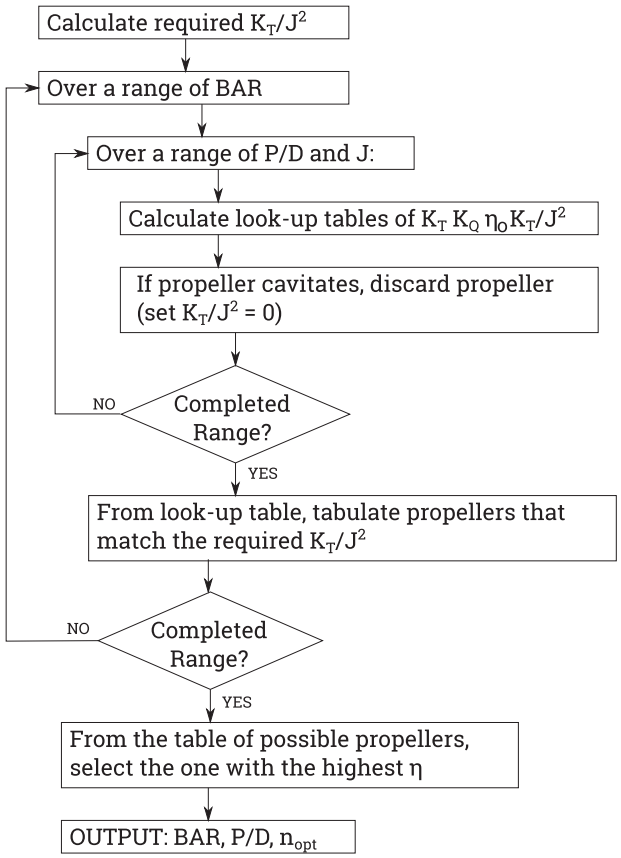

Fig. 7. Propeller selection algorithm.

$$K_T = \frac{T}{\rho n^2 D^4}$$
$$J = \frac{Va}{nD}$$
$$\frac{K_T}{J^2} = \frac{T}{\rho V_a^2 D^2} \tag{22}$$

Referring to Fig. 7 a scheme to calculate the optimum propeller is described as follows: the Blade Area Ratio (*BAR*) is incremented from 0.3 to 1.5. For each value of *BAR*, K_T, K_Q, $\frac{K_T}{J^2}$ and open-water efficiency, η_o, are calculated over a range of J and P/D, and recorded in an array. Each propeller in the array is then checked for excessive cavitation. In the case of the *OOVOO* propeller model, cavitation checks are performed from formulae derived from charts developed by Burrill (1963) with a limit of 5% back cavitation. In the case of the unsteady *CBEMT* propeller model, cavitation criteria are obtained from the empirical formulae developed by Shen and Fuhs (1999), with a limit of 5% back cavitation. If the propeller is found to cavitate excessively, then it is rejected by setting the value of $\frac{K_T}{J^2}$ to zero.

Once a table of propeller characteristics has been generated over a range of J and P/D, for the particular value of *BAR* an array is populated containing possible propeller parameters that match the *required* value of $\frac{K_T}{J^2}$.

When the *BAR* has reached its final increment, the propeller with the highest efficiency is selected from the array of possibles.

The methodology for selecting a propeller, either accounting for or neglecting oblique inflow, remains the same, following that of Fig. 7. This ensures there is no bias from the selection routine

Table 1
Example of convergence of design and in-service propeller efficiency using the algorithm of Fig. 7.

Characteristic	Iteration 1 Optimised propeller selection	Iteration 2 Optimised propeller selection
Design conditions		
Drift angle	0.0 (deg)	1.285 (deg)
Number of propellers	1	1
Number of blades	5	5
Diameter	7.90 (m)	7.90 (m)
Pitch	6.29 (m)	9.25 (m)
Expanded Blade Area ratio	0.667	0.471
Optimum revolutions	114.60 (rpm)	90.57 (rpm)
Optimum efficiency	0.721	0.656
Operational conditions (with environmental loading)		
Drift angle	1.285 (deg)	1.285 (deg)
Revolutions	120.812	90.662
Efficiency	0.640	0.656

itself.

For the analysis carried out in this study, the propeller's diameter remains fixed at the maximum size for the ship's aperture, to maximise efficiency from standard B-Screw propeller. The number of blades is also chosen to remain as the original design, so as to minimise unwanted blade/shaft harmonics from the unchanged engine.

To illustrate the procedure outlined above, Table 1 shows an example output from the algorithm of Fig. 7 when run within the *SiS* simulator. To obtain a basis design, Iteration 1 is chosen from the calm-water, OOVOO model, from which the second propeller model can be chosen from the unsteady MBEMT method. The example is of the *KCS* at 20 knots with a beam wind of 15 knots. This shows the convergence of the design and in-service propeller efficiency from the key driving parameters.

4.2. Case study development

Two different basis ship types were investigated in the analysis. One, the *Esso Osaka*, which was a 25,7145 ton DWT Very Large Crude Carrier (VLCC), and the other, the KRISO Container Ship (KCS) which is a 3600 TEU Container ship concept design.

The KCS was conceived to provide data for both explication of flow physics and CFD validation for a modern container ship with bulb bow and stern (ca. 1997). No full-scale ship exists (SIMMAN, 2014).

These two basis ships were chosen as they have very different manoeuvring behaviour and have both been rigorously studied by numerous research institutes (SIMMAN, 2014; ITCC, 2002). The container ship has a full scale design speed of 24 knots, whereas the fuller bodied VLCC had a service speed of 12 knots. Table 2 shows the main dimensions of both the *Esso Osaka* and the *KCS*. The Body Plans can be seen for each ship in Figs. 8 and 9.

In order to determine any potential propeller efficiency gain from accounting for a ship's manoeuvring motion when selecting a propeller, the following methodology has been developed.

- A first simulation is run. This run selects an optimised propeller using a propeller model which neglects the effects of oblique inflow (the *OOVOO* model).
- A second simulation is run. This time an optimised propeller is selected from a propeller model which accounts for oblique inflow (the modified *CBEMT* model).

Table 2
Main particulars of the *Esso Osaka* and the *KCS*.

Particulars	*KCS* (container ship)	*Esso Osaka* (*VLCC*)
$L_{pp}(m)$	230.0	325.0
$L_{wl}(m)$	232.5	335.0
$B_{wl}(m)$	32.2	53.0
$T(m)$	10.8	21.79
$\nabla(m^3)$	52,030	311,902
C_B	0.651	0.831
C_M	0.985	0.990
L_{CB} (%), fwd+	−1.48	3.169
No. of blades	5	5
$D(m)$	7.9	9.1
$P/D(0.7R)$	0.997	0.715
a_E	0.800	0.682

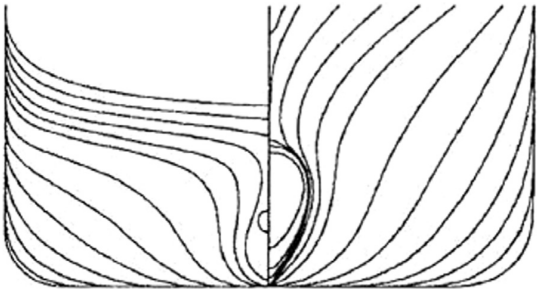

Fig. 8. Body plan of KCS.

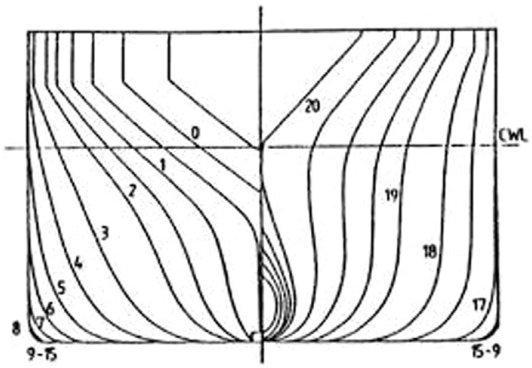

Fig. 9. Body plan of Esso Osaka.

- A third simulation is run. This is an analysis run, not an optimisation one. It analyses the performance of the propeller selected in the first run, while modelling the effects of oblique flow.

The difference between the second run and the third run gives potential efficiency gains from accounting for the effects of a ship's manoeuvring motion due to her environment.

The above procedure is run for each basis ship type. Throughout each simulation run, the environmental conditions are kept constant (a fresh breeze of 20 knot, or Beaufort Number 5, over the port beam), and each ship type has identical courses, i.e. the relative environmental loading on each ship is the same.

Table 3 summarises the case studies analysed.

5. Results, analysis and discussion

It should be noted that during the simulation, at time $t=0$, the forces and moments from the environment are instantaneously

Table 3
Case studies for propeller selection analysis.

Case number	Description
1	*Esso Osaka*, basis propeller is selected based on *OOVOO* model
2	*Esso Osaka*, basis propeller is selected based on unsteady modified *CBEMT* model
3	*Esso Osaka*, basis propeller selected from Case 1 is run using the modified *CBEMT* unsteady propeller model and analysed
4	Identical to case 1, except run on the *KCS*
5	Identical to case 2, except run on the *KCS*
6	Identical to case 3, except run on the *KCS*

applied to the particular ship in question. This will result in an initial transient that will settle down, once the automatic pilot and speed control have re-established the set point.

In order to avoid biasing the outcome from autopilot behaviour, the results that occur between the end of the initial transient and the end of the run are used for further analysis. After running the simulator, the output shows there is a gain in open-water propeller efficiency of 1.761% for the *Esso Osaka*, when the propeller has been selected when accounting for manoeuvring motion, compared to neglecting it.

Similarly, there is a gain in open-water propeller efficiency of 2.340% for the *KCS*, when the propeller has been selected when accounting for manoeuvring motion, compared to neglecting it.

The specific fuel consumption (SFC) of an engine will vary depending on whereabouts in the engine load diagram the operating point is. This operating point will vary dynamically as the engine load varies throughout the course of the ship's voyage. To obtain an accurate forecast of fuel consumption and emissions output, it is necessary to incorporate a sophisticated engine simulator into the manoeuvring simulator, the scope of which is beyond this study.

To simplify the fuel and emissions calculations, it is assumed that the mean quasi-steady main engine's brake power results in the mean quasi-steady values for fuel consumption and CO_2 emissions.

To calculate the CO_2 emissions from a fuel, the Carbon content of the fuel must be multiplied by the ratio of molecular weight of CO_2 to the molecular weight of *C*, that is 44:12.

The Carbon content of Heavy Fuel Oil (HFO) (ISO 8217 Grades RME through RMK) have a Carbon content of 84.93%, therefore, 1 g of HFO produces $0.8493 \times \frac{44}{12} = 3.1141$ grammes of CO_2 when fully combusted.

If it is assumed that the specific fuel consumption vs brake engine power output trend is similar to all slow-speed engine manufacturers, that is, constant over the range of brake power from the different case studies, then the comparative differences in fuel consumption between case studies are independent of the value of SFC, and therefore engine manufacturer.

To give an indication of computational resources, when the *SiS* simulator has been compiled with debug symbols and gfortran v5.3.1, using the OpenMP shared-memory parallel programming library, the total CPU time in user space is 7.692 s. This relates to a simulation lasting 47 real minutes using the *OOVOO* model for optimisation. Using the *MBEMT* for optimisation takes a total CPU time in user space of 52,231.120 s. Upon profiling the code, much of the time is used within the minimisation algorithm used to calculate induced velocities inside the *BEMT*. The CPU time can vary dramatically, depending upon input parameters (excluding real simulation time), indicating that the minimisation algorithm finds certain conditions considerably more challenging to solve than others.

5.1. Main input parameters and assumptions

The main input parameters used in the simulation routines include ship particulars necessary to satisfy calm-water resistance calculations (Holtrop and Mennen, 1982; Holtrop, 1984). Rudder dimensions are required to assess the response of the ship's motions to the helm/autopilot/environment. True wind velocity and windage areas of the ship are required to estimate environmental forces and moments. Values for wind speed and direction can be obtained from sources such as NOAA (2016). The Ship's course is also an input parameter, so as to be able to calculate relative environmental forces and moments, and also allow the autopilot to operate as desired. The autopilot's PID parameters are also input variables, which are tuned for each particular ship in question.

When used as an analysis tool to examine existing designs, principal propeller dimensions such as diameter, pitch, blade-area-ratio and number of blades are also required (which can be obtained from the *SiS* simulator in *design* mode).

It is assumed in this analysis that there is only one leg in the voyage, with the ship's course due North. In practice the voyage would be split up into different legs, where the ship's course or prevailing weather conditions are predicted to be significantly different, then for each particular leg select an optimum propeller. Finally, simulations are run for the whole voyage with every propeller selected from each leg, enabling the most efficient propulsion solution overall to be chosen.

The analysis procedure currently neglects alterations in the propeller's wake-field due to the hull, and as such will be more precise for ships whose hullforms do not greatly alter the propeller's wake-field. A hullform whose tendency is to alter the inflow may result in increased unsteadiness due to augmented asymmetry from greater oblique flow on one side compared to the other, when sailing at some drift angle. This requires further experimentation, however, this being the case, it would imply that the use of the presented propeller selection methodology can potentially yield higher efficiency gains.

A further assumption is that the propeller chosen from the optimisation processes (based upon the Wageningen B-Screw) does not result in adverse structural problems.

5.2. Esso osaka

A Wärtsilä RTA82T is chosen as an example of an engine that has the necessary requirements to satisfy the propulsion of the *Esso Osaka*. The specific fuel consumption is regarded to be a constant of 166 g/kW h (Wärtsilä, 2013) over the range of brake power output from the case studies. This fuel consumption can be equated to grammes of CO_2 produced per kW h, viz.

CO_2 produced/kW h = $166 \times 3.1141 = 516.94$ g/kW h

Table 4 summarises the fuel consumption and CO_2 emissions from the cases described in Table 3 for the *Esso Osaka*. The saving in fuel for the *Esso Osaka* from selecting an optimum propeller for in-service conditions using an unsteady modified *CBEMT* model compared to the "dead ahead" *OOVOO* model (and run in service conditions) is 1.780%. The corresponding CO_2 emissions savings 1.765%.

5.3. KRISO container ship – KCS

An RTA82C from Wärtsilä is chosen as an example of an engine that has the necessary requirements to satisfy the propulsion of the *KCS*. The specific fuel consumption is regarded to be a constant of 170 g/kW h (Wärtsilä, 2013) over the range of brake power output from the case studies. This fuel consumption can be

Table 4
Fuel consumption and CO_2 emissions for the *Esso Osaka*.

	Case number		
Characteristic	1	2	3
Required $P_B(kW)$	7696.89	7645.53	7782.29
Fuel consumption (t/h)	1.278	1.269	1.292
CO_2 produced (t/h)	3.979	3.952	4.023

Table 5
Fuel consumption and CO_2 emissions for the *KCS*.

	Case number		
Characteristic	4	5	6
Required $P_B(kW)$	40,120.27	38,040.02	39,302.24
Fuel consumption (t/h)	6.820	6.467	6.681
CO_2 produced (t/h)	21.240	20.138	20.807

equated to grammes of CO_2 produced per kW h in an identical manner to that for the *Esso Osaka*.

$$CO_2 \text{ produced/kW h} = 170 \times 3.1141 = 529.40 \text{ g/kW h}$$

Table 5 summarises the fuel consumption and CO_2 emissions from the cases described in Table 3 for the *KCS*.

The saving in fuel for the *KCS* from selecting an optimum propeller for in-service conditions using an unsteady modified *CBEMT* model compared to the "dead ahead" *OOVOO* model (and run in service conditions) is 3.203%. The corresponding CO_2 emissions savings 3.215%.

6. Conclusions

The overall aim of this research is to reduce the amount of Carbon Dioxide (CO_2) produced from operating ships. The approach taken by the authors to address this aim is to increase the efficiency (and thereby reduce fuel consumption and emissions) by selecting a propeller whose design-point better represents the conditions in which it is expected to operate.

Conventionally, a propeller is selected on the assumption that a ship is sailing with zero drift angle. When a ship is in her natural environment it is likely that when she is full-away on passage, she will have attained some drift angle due to environmental forces and moments imposed on her.

A methodology has been presented to account for the unsteady effects of manoeuvring motion on the propeller selection process. This details the effects of a ship's motion and propulsion system response due to environmental loading. Case studies were developed which show how the efficiency of a propeller fairs from the newly proposed method of propeller selection, compared to conventional methods.

Two ship types have been examined, a VLCC, the *Esso Osaka*, and a container ship, the *KCS*. The *Esso Osaka*'s open water propeller efficiency increased by 1.76%, from using the newly proposed propeller selection method, and the *KCS*'s open water propeller efficiency increased by 2.34%. This equates to a saving in CO_2 emissions for the *Esso Osaka* of 1.77% and 3.22% for the *KCS*.

The results suggest that the more susceptible a ship is to drift, the higher the potential efficiency gains from the newly proposed propeller selection method.

From further analysis of results, it is shown that if a ship has a relatively high required power, seemingly small increases in propeller efficiency can manifest itself as a large CO_2 emission reduction, and noticeable reductions in fuel consumption.

The results of this work show potential for reducing a ship's CO_2 emissions by using a propeller selection method which accounts for the manoeuvring motion of a ship, that is, a design which accounts for a ship's motion response to an environment in which she is expected to operate.

As a consequence of running this type of analysis, it is observed that an estimate for the sea-margin is naturally obtained as an output. Using a simulator at the initial design stages can, therefore, conceivably produce values with a higher degree of accuracy compared to more traditional "rule of thumb" approaches.

A ship simulator can be used as a valuable tool at the initial design stage, not only for analysing a ship's motions, but as a method of obtaining more realistic loading estimates (and therefore design-points) for a ship in her natural environment, rather than the usual synthetic calm-water plus sea-margin.

Finally, it must be noted that this research is considered to be in the initial, proof-of-concept stages of development. Actual values given in the results are expected to differ from physical experiments due to various simplifying assumptions, however, inferences drawn and general outcome and conclusions are not expected to differ from physical experiments.

Acknowledgements

The authors wish to thank the Engineering and Physical Sciences Research Council (EPSRC), reference EP/H019871/1, for sponsoring this work.

References

Abbott, I.H.A., Von Doenhoff, A.E., 1959. Theory of Wing Sections: Including a Summary of Airfoil Data. Courier Dover Publications, New York.
Abkowitz, M.A., 1964. Lectures on Ship Hydrodynamics – Steering and Maneuverability. Technical Report HY-5, Hydro and Aerodynamic's Laboratory. Lyngby, Denmark.
Beddoes, T., 1976. A synthesis of unsteady aerodynamic effects including stall hysteresis. Vertica 1, 113–123.
Bisplinghoff, R., Ashley, H., Halfman, R., 1996. Aeroelasticity. Dover Books on Aeronautical Engineering Series. Dover Publications Inc, New York, USA.
Blendermann, W., 1996. Wind Loading of Ships – Collected Data from Wind Tunnel Tests in Uniform Flow. Technical Report 574, Institut für Schulungsmaßnahmen, University of Hamburg.
Burrill, L. C., 1963. Propeller Cavitation: Further Tests on 16 in. Propeller Models in the Kings College Cavitation Tunnel. Transactions of The North East Coast Institution of Engineers and Shipbuilders.
Carlton, J., 1997. Marine Propellers and Propulsion, 2nd edition. Butterworth Heinemann, Oxford, UK.
Coleman, R., Feingold, A., Stempin, C., 1945. Evaluation of the Induced Velocity Field of an Idealized Helicopter Rotor. Technical Report ARR No. L5E10, National Advisory Committee for Aeronautics.
Davenport, A.G., 1978. Wind structure and wind climate. In: International Research Seminar on Safety of Structures under Dynamic Loading. Norwegian Institute of Technology, Trondheim, pp. 209–237.
Drela, M., 2013. Xfoil, ⟨http://web.mit.edu/drela/Public/web/xfoil/⟩ (accessed 13.01.2016).
Dubbioso, G., Muscari, R., Di Mascio, A., 2013. Cfd analysis of propeller performance in oblique flow. In: Third International Symposium on Marine Propulsors, SMP'13. CNR-INSEAN, CNR-IAC, Launceston, Tasmania, Australia, pp. 298–305.
Francis, M.S., Keesee, J.E., 1985. Airfoil dynamic stall performance with large amplitude motions. AIAA J. 23.
Glauert, H., 1928. On the Horizontal Flight of a Helicopter. Technical Report 1157, British Aeronautical Research Council: Reports & Memoranda.
Goldstein, S., 1929. On the vortex theory of screw propellers. Proc. R. Soc. Lond. Ser. A 123, 440–465.
Green, R., Galbraith, R.A., 1994. A demonstration of the effect of the testing environment on unsteady aerodynamics experiments. Aeronaut. J. 98.
Harvald, S., 1967. Wake and Thrust Deduction at Extreme Propeller Loadings. Technical Report, Publications of the Swedish State Shipbuilding Experimental Tank, Nr. 61.
Hirano, M., 1981. A practical calculation method of ship maneuvring motion at initial design stage. Nav. Arch. Ocean Eng. 19.

Holtrop, J., G., Mennen, 1982. An approximate power prediction method. Int. Shipbuild. Prog. 29, 166–170.
Holtrop, J., 1984. A statistical re-analysis of resistance and propulsion data. Int. Shipbuild. Prog., 272–276.
Inoue, S., Hirano, M., Kijima, K., Takashina, J., 1981. A practical calculation method of ship manoeuvring motion. Int. Shipbuild. Prog. 28.
ITTC, 2002. The specialist committee on esso osaka – final report and recommendations to the 23rd ittc. In: 23rd ITTC, International Towing Tank Conference.
Kerwin, J., Kinnas, S., Lee, J., Shih, W., 1987. A surface panel method for the hydrodynamic analysis of ducted propellers. Trans. SNAME 95, 93–122.
Kose, K., Yumuro, A., Yoshimura, Y., 1981. Concrete of mathematical model for ship manoeuvrability. In: 3rd Symposium on Ship Manoeuvrability, Society of Naval Architects of Japan (in Japanese).
Kottapalli, S.B., Pierce, G.A., 1979. Drag on an oscillating airfoil in a fluctuating free stream. Fluids Eng. 101.
Lee, T., Ahn, K., Lee, H., Yum, D., 2003. On an empirical prediction of hydrodynamic coefficients for modern ship hulls. In: MARSIM'03. Hyundai Heavy Industries Co., Ltd, Korea.
Leishman, J.G., Beddoes, T.S., 1989. A semi-empirical model for dynamic stall. Am. Helicopter Soc. 34 (3), 3–17.
Leishman, J.G., 1989. Two-dimensional model for airfoil unsteady drag below stall. J. Aircr. 25 (7).
Leishman, J., 2002. Principles of helicopter aerodynamics, Cambridge Aerospace Series. Cambridge University Press, Fairfax, USA.
Li, Z., Zhang, G., He, W., van Terwisga, T., 2015. A numerical study of unsteady cavitation on a hydrofoil by LES and URANS method. J. Phys. Conf. Ser. 656(1), 012157.
McCroskey, W.J., 1981. The Phenomenon of Dynamic Stall. Technical Report, TM 81264, NASA.
McLaughlin, T.E., 1992. Aerodynamic Foundations for Use of Unsteady Aerodynamic Effects in Flight Control (Ph.D. thesis). University of Colorado, Department of Aerospace Engineering Sciences.
MEPC, 2014. Reduction of GHG Emissions from Ships, Third IMO GHG Study 2014 Final Report. Technical Report, MEPC 67/INF.3, Marine Environment Protection Committee, London, UK.
NOAA, 2016. Blended Sea Winds, ⟨https://www.ncdc.noaa.gov/data-access/marineocean-data/blended-global/blended-sea-winds⟩ (accessed 02.02.2016).
Oltmann, P., Sharma, S., 1984. Simulation of Combined Engine and Rudder Maneuvers Using an Improved Model of Hull–Propeller–Rudder Interactions. Technical Report 444, Technische Universität Hamburg-Harburg, Hamburg (prepared for the Fifteenth ONR Symposium on Naval Hydrodynamics).
Oosterveld, M., van Oossanen, P., 1975. Further computer-analysed data of the wageningen b-screw series. Int. Shipbuild. Prog. 22.
Shen, Y., Fuhs, D., 1997. Blade Section Lift Coefficients for Propellers at Extreme Off-design Conditions. Technical Report, CRDKNSWC/HD-1205-02, Hydrodynamic Directorate Research and Development Report, Naval Surface Warfare Centre, Carderock Division.
Shen, Y., Fuhs, D., 1999. Dynamic Effects on Propellers Blade Section Lift, Drag, and Pitching Moment Coefficients. Technical Report, CRDKNSWC/HD-1205-0, Hydrodynamic Directorate Research and Development Report, Naval Surface Warfare Centre, Carderock Division.
SIMMAN, 2014, ⟨http://www.simman2013.dk/⟩ (accessed 19.04.2014).
Son, K., 1989. On the mathematical model for estimating the manoeuvring performance of ships. Soc. Korea Voyag. 13 (2).
Stettler, J., 2004. Steady and Unsteady Dynamics of an Azimuthing Podded Propulsor Related to Vehicle Maneuvering (Ph.D. thesis). Massachusetts Institute of Technology.
Townsin, R.L., Kwon, Y.J., Baree, M.S., Kim, D.Y., 1992. Estimating the influence of weather on ship performance. Trans. RINA 135, 191–209.
Trodden, D.G., 2014. Optimal Propeller Selection When Accounting for a Ship's Manoeuvring Response due to Environmental Loading (Ph.D. thesis). School of Marine Science & Technology, Newcastle University, UK.
Wärtsilä, 2013. General Technical Data for Wärtsilä Marine Low-speed Engines, ⟨http://www.wartsila.com/en/marine-solutions/products/netGTD⟩ (accessed 18.12.2013).
World Trade Organization, 2013. International Trade Statistics 2013.
Yoshimura, Y., 2005. Workshop on Mathematical Models for Operations Involving Ship–Ship Interaction. August 2005 Tokyo, Technical Report, Hokkaido University.
Young, Y., Kinnas, S., 2001. A bem for the prediction of unsteady midchord face and/or back propeller cavitation. Fluids Eng. 123, 311–319.